Journal of
Ceramic Science
and Technology

The Influence of the Coarse Fraction on the Porosity of Refractory Castables

J. Fruhstorfer[*], C.G. Aneziris

Institute of Ceramic, Glass and Construction Materials, Technische Universität
Bergakademie Freiberg, Agricolastraße 17, 09596 Freiberg, Germany

Abstract

In this work, the influence of the coarse fraction of a particle size distribution on the flowability and density of refractory castables is investigated. A modified Andreasen model was developed to combine distribution moduli ≤ 0.30 in the fine fraction for flowability and stability with moduli adjusted between 0.28 and 1.20 in the coarse fraction for improving density. The amount of the fine fraction was held constant. It was shown that a density-optimized batch showed self-flowing behaviour, while the other batches needed to be vibrated. The bulk density of the unfired and fired ceramics was measured. The castable showing the best flowability with a distribution modulus of 0.80 in the coarse fraction also had the highest density and the smallest pore sizes with regard to the full range of pores. The pore sizes were measured by means of mercury porosimetry, optical microscopy and a visual method owing to the large range of pore sizes.

Keywords: Refractory castables, coarse fraction, flowability, density, pore size distribution

I. Introduction

High-performance castables have been extensively studied owing to the increasing importance of monolithic refractories in steelmaking. The relative consumption of shaped refractory bricks is continuously decreasing, while the amount of monolithic refractories is increasing as shown in Fig. 1 [1,2,3]. This relative change is mainly a result of an increased use of monolithics in steel secondary metallurgy, for example in steel ladle linings [1,4].
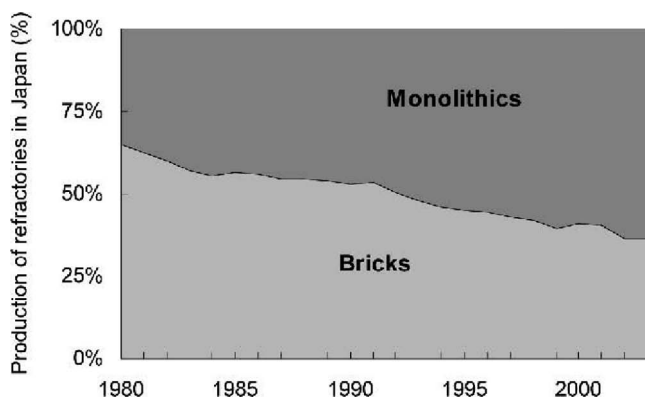

Fig. 1: Relative consumption of bricks and monolithic refractories in 2003 in Japan [2]

A central problem in designing an unshaped refractory is the simultaneous optimization of the interrelated properties stability, flowability and density [5,6,7,8]. In this optimization the particle size distribution plays a key role [9]. Particle size distributions of coarse refractories consist of fine particle fractions < 0.1 mm, medium grain sizes between 0.1 and 1 mm and coarse grain fractions > 1 mm [10].

In general, particle size distributions can be designed to be discrete or continuous [11]. The blending of discrete particle sizes to achieve a high packing density was first described by Furnas [12]. In that packing model the finer particles fit into the interstices of the coarser particles for a diameter ratio of about 7 [11]. Andreasen [13,14] introduced a continuous packing model as presented in Equation 1. Densest packing of granular materials was determined for a distribution modulus n between 1/3 and 1/2. Dinger and Funk [14] modified the Andreasen model recognizing a finite minimum particle diameter and found on the basis of numerical calculations that optimal dense packing of ideal spheres was achieved for a distribution modulus of 0.37 [15]. Zheng *et al.* [16] explained that every single size class used for designing a particle size distribution has a specific distribution modulus which depends on the particle size ratio and the interstitial pore fraction of each class. The differences of the moduli for different size classes were explained based on differing grain properties like, for example, grain morphology.

$$A_v(d) = 100\ \% \times \left(\frac{d}{d_{max}} \right)^n \qquad (1)$$

with

d	particle diameter in mm
$A_V(d)$	cumulative percent finer than d in %
d_{max}	maximum particle diameter in mm
n	distribution modulus

For different forming technologies, different particle size distributions are favored owing to the interrelation of the

* Corresponding author: jens.fruhstorfer@ikgb.tu-freiberg.de

particle size distribution with other properties. Table 1 shows a short overview of ceramic shaping technologies with the assigned distribution moduli. Another important property for slip casting and spray drying is, for example, the dewatering ability besides the density of the particle size distribution. Batches for plastic forming should have a good flowability under pressure [17]. For dry pressing, density-optimized distributions are applied, theoretically with a modulus of 0.37 [15]. However, for practical densest packings, the value of the modulus can exceed 0.5 [11]. More recently, experiments on the densest distributions of dry-pressed alumina-zirconia-graphite refractories with a maximum particle size of up to 1 mm conducted by Yu et al. [18] showed distribution moduli between 0.8 and 0.9 for optimum packing. The differences between the moduli could be explained based on different grain properties like size and morphology as supposed by Zheng et al. [16] for different size classes. For refractory castables the assigned distribution moduli range from values adjusted for slip casting to values used for dry pressing. The reason is the complex optimization of the interconnected properties flowability, stability and density. Depending on the application and the favored properties, the modulus could be adjusted. Therefore in the following, the properties and interrelations of castables are described in more detail.

Table 1: Shaping technologies and assigned distribution moduli n.

Shaping technology	Dist. modulus	Source
Slip casting and spray drying	0.19 – 0.21	17
Plastic forming	0.20 – 0.26	17
Refractory castables	0.2 – 0.3	7
	0.22 – 0.26	8
	0.26	4
	0.28 – 0.30	5
	0.32 – 0.42	17
	0.3 – 0.7	19
Dry pressing	0.33 – 0.5	13
	0.37	17
	> 0.5	11
	0.8 – 0.9	18

The viscosity as a characteristic of the flowability of a slip or castable depends on the fluid, the particle size distribution, the solid content and the particle interactions [20,21]. Sudduth [20,22,23] described a generalized model to predict the apparent viscosity of solutions. The model and experimental results showed high agreement. To summarize, a density-optimized distribution shows a lower viscosity than a non-optimized one for equivalent solid contents in the suspensions, although the particle interactions also increase with the packing optimization. Working on the basis of this generalized model, Amaral [21] examined how the viscosity also decreased with an increasing width of the particle size distribution. For bimodal particle size distributions with a size ratio of large to small particles of 10 or higher, Farris [24] found that the apparent viscosity increased with the solid content for constant size distributions. Anyway there is a minimum of the viscosity depending on the particle size distribution. The location of the minimum viscosity was found for a coarse fraction of the total filler content of ≈ 65 % for solid contents up to 75 %. Additionally, Hoffman [25] observed that the location of the minimum viscosity for suspensions containing submicron particles in a bimodal size distribution tends to be shifted towards particle mixtures containing a greater amount (≥ 70 %) of large particles owing to the strong viscosity-increasing effect of submicron particles.

Besides the apparent viscosity, the yield stress influences the flowability. The yield stress also ensures the stability of the coarse fraction of the castable [26]. Pivinskii [26] identified that colloidal powder additions to comparatively coarse slips retard the settling of the coarse particles. According to Dzuy [27], the particle interactions are the cause of the yield stress. Consequently, the yield stress like the viscosity depends on the solid content in a suspension. Moreover Rhines [28] correlated the particle contact points and therefore the particle interactions with the apparent density for granular materials. With an increasing apparent density as provided by densest packing, particle contacts also increased. Thus flowability, stability and density interact.

Investigations on the behaviour of castables considering the interactions between flowability, stability and density were recently conducted. For example Silva [8] discovered for stable castables that the fine fraction strongly influences the rheological properties and acts as a lubricant for the coarse fraction. The highest flowability was observed for distribution moduli between 0.22 to 0.26. In that study, density was not taken into account. The influence of the addition of microsilica and therefore of a decreasing minimum particle size was researched by Myhre [7]. It was pointed out that a distribution modulus increasing from 0.2 to 0.3 caused decreasing flowability for stable castables. The flowability of a castable with a distribution modulus of 0.3 significantly increased with the addition of 5 % microsilica. Feys et al. [6] investigated the reason for flow or friction behaviour of stable castables when pumping through a pipe. That study showed that the fine fraction acted like a lubrication layer, significantly reducing friction between the pipe and the concrete. Consequently, the best effect was achieved when also the coarse particles in the castable were separated by the lubrication layer of the fine fraction. Tomsu and Ulbricht [5] also described the lubrication effect of the fine fraction. Moreover it was found that particle size distributions with moduli between 0.28 and 0.30 led to comparatively dense and stable castables with a good flowability.

The previously summarized investigations focused on the optimization of the fine fraction, ensuring a lubrication layer to achieve castables with good properties. Although flowability, stability and density criteria were interrelated, little attention has been paid to the influence of the coarse fraction on the properties and behaviour of a castable. However, for refractory applications especially

the combination of the fine and coarse fraction in a particle size distribution is important owing to the influence on the thermomechanical properties, for example, on thermal shock resistance [19, 29, 30]. The fine particle fraction causes shrinkage when thermally treated and the development and opening of cracks between the larger particles. Hence a microcrack network is induced which significantly increases the resistance to thermal shock [30].

The purpose of this study therefore is to investigate the influence of the coarse fraction on the castable properties. Based on the Andreasen model, it was shown that good flowability was achieved for distribution moduli ≤ 0.30, but densest packing for distribution moduli ≥ 0.37. An approach for a simple design for a castable particle size distribution which solved this contradiction was developed and a simple model derived. The input for this new model is, in addition to the maximum particle size, one distribution modulus defining the fine particle fraction and a second one describing the coarse fraction. The stability of the aggregates is provided by a constant fines content with a distribution modulus between 0.28 and 0.30. For the coarse particle fraction different packings were investigated based on the use of different distribution moduli. The best-flowing and densest castable was achieved with a distribution modulus of 0.80 for the maximum grain size in the coarse fraction.

II. Experimental

The current study involves analyzing the used alumina fractions, dispersant experiments and investigating the effect of the coarse fraction on the castable properties flowability and density for stabilized vibrated castables. The influence of the coarse fraction was investigated for a constant water content and a constant flowability which was adjusted carefully based on the amplitude of a vibrating table.

The raw materials were alumina fractions up to 3 mm, a binder, a defoamer, a dispersant and water. Tabular aluminas (Tabular Alumina T60/64, Almatis GmbH, Germany) and reactive alumina (CL370, Almatis GmbH, Germany) were used. The particle size distributions of the aggregates were measured for calculating the amounts to use according to a new model approach. The size distributions of the fractions < 0.5 mm were measured with laser granulometry (Beckmann Coulter LS 230) and a previous deagglomeration treatment in an ultrasonic bath for 5 minutes according to the standard DIN EN 725 – 5. The particle size distributions of coarser fractions were sieve-analyzed according to the standard DIN 66165 – 2. The true densities of the fractions were investigated with a helium pycnometer (Accupyc 1330, Micromeritics GmbH, Germany) in compliance with DIN 66137 – 2. The measured values are listed in Table 2. The additives used were a re-hydratable alumina binder (Alphabond 300, Almatis GmbH, Germany), a non-ionic defoamer (Contraspum K 1012, Zschimmer & Schwarz GmbH & Co. KG, Germany) and a dispersant based on polyethylene glycol (Castament FS 60, BASF Construction Polymers GmbH, Germany).

Table 2: Raw material properties.

Material	Tabular Alumina T60					CL370	Alphabond 300
Fraction in mm	1 – 3	0.5 – 1	0 – 0.5	0 – 0.2	0 – 0.02		
Sieve s in μm	Retention of sieve s in wt%						
0.1	0	0	0	3.96	19.40	32.40	3.75
0.4	0	0	0	3.01	14.70	40.30	4.81
1	0	0	0	5.53	22.40	27.30	24.04
4	0	0	0	7.40	16.40	0	31.50
10	0	0	0	22.90	19.00	0	35.90
40	0	0	0	21.90	1.30	0	0
90	0	0	22.82	19.50	1.30	0	0
150	0	0.20	24.49	14.80	5.45	0	0
315	0.07	15.49	48.78	1.00	0.05	0	0
630	2.76	79.22	3.91	0	0	0	0
1000	6.60	4.89	0	0	0	0	0
1250	32.89	0.2	0	0	0	0	0
2000	25.53	0	0	0	0	0	0
2500	28.84	0	0	0	0	0	0
3150	3.31	0	0	0	0	0	0
density in g/cm^3	3.649	3.678	3.800	3.884	3.919	4.013	2.781

The compositions of the castables were based on a modified Andreasen model. In contrast to the standard model [13] where the distribution modulus is constant and independent of the particle size, the new approach applies a modulus dependent on the particle size. Good flowability and stability of castables is attained for distribution moduli of the fine fraction between 0.28 and 0.30 as described by Tomsu and Ulbricht [5] for the conventional model. By applying a variable distribution modulus like Zheng *et al.* [16], it is possible to define a modulus equation. In this study a simple linear model as shown in Equation 2 was chosen. The modulus equation depends on the grain size d and on two constants. The two constant parameters are the modulus at the maximum grain size n_{max} and the one for an infinite small size n_{min}, respectively. The final modified model is presented in Equation 3. The defined maximum grain size of all prepared castables was $d_{max} = 3150$ μm. The minimum distribution modulus n_{min} was chosen to be 0.28 because then n(d) ranges between 0.28 and 0.30 in the fine fraction. Therefore a good flowability and stability should be ensured. The maximum modulus n_{max} was adjusted between 0.28 and 1.20 to investigate the influence of the coarse fraction on density and flowability. The parameters and the modified model are empirical and depend on the maximum and minimum particle size. The evolution of the distribution modulus n(d) as a function of the particle size d is shown in Fig. 2. For the calculation of the compositions listed in Table 3 the differing true densities of the materials and fractions were considered. It can be seen that a varying n_{max} does not affect the amount of fine fractions constituting the matrix ≤ 100 μm, but can be used as the describing parameter for the different coarse fractions. The total errors are also listed in Table 3. These are the sums of the squared deviations between the ideal modified Andreasen curves and the ones of the real mixtures for each sieve class as listed in Table 2. Values of the total error ≤ 150 appeared to be sufficient regarding the fitting of the ideal and the real curve. This method of calculating the total error is in line with that of Klippel *et al.* [31], in which the sums of the absolute values of the deviations were calculated. However, if the squared values are summed up instead of the absolute ones, the total error is more sensitive to high deviations. The defoamer was added in an amount of 0.1 wt% as recommended by the supplier. The water addition for all experiments was 5 wt%.

$$n(d) = n_{min} + d \cdot \frac{n_{max} - n_{min}}{d_{max}} \qquad (2)$$

with

d — particle diameter in mm
n(d) — dist. modulus dependent on d
d_{max} — maximum particle size in mm
n_{max} — dist. modulus for max. particle size
n_{min} — dist. modulus for min. particle size

$$A_V(d) = 100\ \% \cdot \left(\frac{d}{d_{max}}\right)^{n_{min} + d \cdot \frac{n_{max} - n_{min}}{d_{max}}} \qquad (3)$$
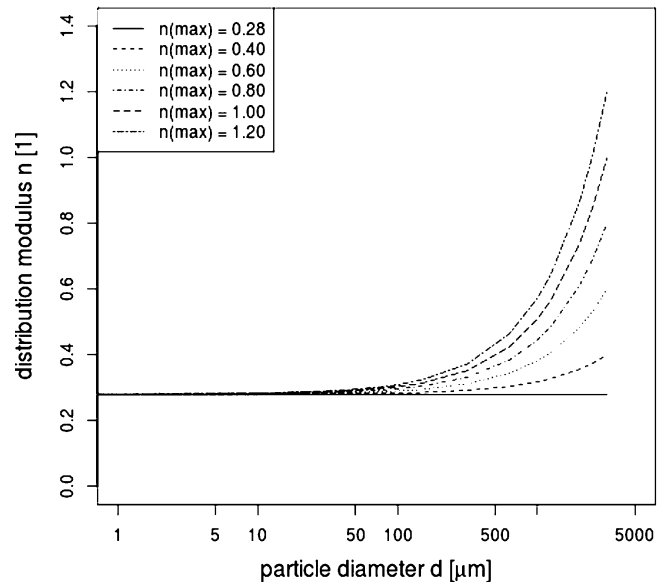

Fig. 2 : Evolution of the distribution modulus n as a function of the particle size d for $n_{min} = 0.28$.

Table 3: Castable compositions with $n_{min} = 0.28$ and varying n_{max}

n_{max}	0.28	0.40	0.60	0.80	1.00	1.20
materials	Mass fraction in wt%					
T60 1 – 3	25	30	35	40	45	50
T60 0.5 – 1	15	10	10	10	5	5
T60 0 – 0.5	15	15	10	5	5	0
T60 0 – 0.2	30	30	30	30	30	30
CL370	12	12	12	12	12	12
Alphabond 300	3	3	3	3	3	3
Total error	77	68	56	62	67	90

The castables were prepared with a concrete mixer (ToniMIX, Toni Baustoffprüfsysteme GmbH, Germany). Prior to being mixed, the fractions were carefully weighed. The batches of 2000 g were dry-mixed for 1 min, water was added and then the batches were wet-mixed for 5 min. After the batches had been mixed, the casting moulds (10 x 10 cm² base area) were filled and then vibrated for 5 min. The amplitude of the vibrating table (JMV 800/1000x800, JÖST GmbH & Co. KG, Germany) was adjusted between 0 mm (no vibration) and 0.55 mm depending on the experiment.

The experiments to identify the optimal addition of dispersant were only conducted for the standard Andreasen model with n = $n_{min} = n_{max} = 0.28$. With this particle size distribution as described in Table 3 and 5 % water addition, no self-flowing castable was obtained, which is in line with the results of Myhre [7]. Instead of adding microsilica like Myhre [7], in this study the masses were vibrated and the minimum amplitude at which flowing started was determined as an indicator for the effect of the dispersant. The tested amounts of the additive were 0.4, 0.5, 0.6, 0.7 and 0.8 wt%.

For investigating the influence of the coarse fraction on the castable properties the optimal dispersant amount of the particle size distribution with $n = n_{min} = n_{max} = 0.28$ was used for all particle size distributions. The masses were prepared the same way as the castables for the dispersant experiments. In a first run of the experiments with the different size distributions, the minimum necessary amplitudes for flowing were determined. In the second run the amplitudes were adjusted such that all batches exhibited the same flowing behaviour. After 1.5 days the casting moulds were removed and the bulk densities were immediately measured based on weighing and measurement of the dimensions.

Heating (Table 4) was performed carefully in the furnace (AGNI FHT 175 – 500, AGNI Wärme- und Werkstofftechnik GmbH, Germany) owing to the strong dehydration of the binder in a small temperature interval. The cast refractories were held at the maximum temperature of 1600 °C for four hours. Cooling was performed at a defined rate of 120 K/h down to 800 °C, after which a free cooling rate was applied.

Table 4: Heating procedure.

ϑ_{start} in °C	ϑ_{end} in °C	Rate in K/h
ϑ_{room}	200	3
200	600	10
600	800	60
800	1600	120

Bulk densities, porosities and pore size distributions of the sintered refractories were measured. From each body, three samples with volumes of $\approx 30\,cm^3$ were cut out to investigate the bulk densities, open, closed and overall porosities according to the standard DIN EN 993 – 1. For the calculation, the true density $3.919\,g/cm^3$ of the alumina fraction 0 – 200 μm (Table 2) was used as it is the finest tabular alumina fraction and therefore it was assumed to have no inner porosity.

The pore size distributions were measured with different methods. With a mercury porosimeter (PASCAL 140/440, Porotec GmbH, Germany), pores to a maximum size of < 150 μm can be detected according to the manufacturer of the porosimeter. Cumulative volume distributions (three-dimensional) were derived according to the standard DIN 66133/ISO 15901 – 1. Larger pores were investigated by means of optical microscopy and visually. With the optical microscope (VHX Digital Microscope 2000, Keyence Microscope Europe, Belgium), the pore areas at a magnification of 20x were detected and maximum and minimum diameter of each pore measured. The results were plotted as cumulative area distributions (two-dimensional) dependent on the average diameter. For the visual measurement the cast bodies were cut and over an area of 40 cm² the pores with sizes ≥ 0.5 mm were counted and measured with a ruler. Discrete classes with mid-values 0.5 mm, 1 mm, 1.5 mm, etc. were used. For this pore size measurement the accuracy was estimated to be ± 0.25 mm. For this da-

ta set, cumulative count distributions (zero dimensional) were generated.

III. Results and Discussion

As outlined in the introduction, the present work investigates the influence of the coarse fraction on the castable properties flowability and density. Therefore a simple model was developed, based on the Andreasen equation. It was described that the maximum distribution modulus n_{max} as a single parameter can define the different coarse fractions of the batches. First the optimal dispersant amount was investigated for the standard Andreasen model with a distribution modulus of 0.28. Subsequently densities and porosities of the unfired and fired ceramics designed according to the new model approach were measured. In a next step the pore size distributions for the full range of pore sizes were determined. Finally, the results were confirmed with optical microscopy images.

Table 2 shows the particle size distributions and the true densities of the used materials considered in the batch calculations. The true densities of the grains decreased with increasing grain size which is in line with the results published by Reed [11] for alumina and by Schafföner et al. [32] for calcium zirconate. The standard and modified Andreasen models are volume distributions and therefore it is important to recognize differences in densities. In the present work, the particle size analysis of each fraction was transformed from the mass distributions as shown in Table 2 to volume distributions, which were used as input for the calculations.
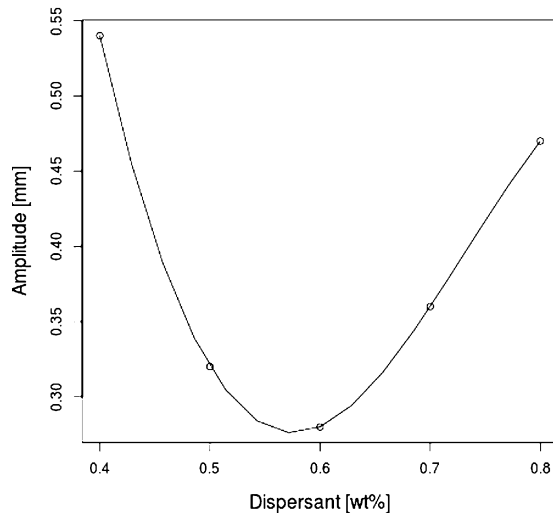

Fig. 3 : Dispersant experiments.

The optimal dispersant amount was measured by determining the minimum necessary vibration amplitude for the beginning of flow. At this point the yield stress was overcome. The results are presented in Fig. 3. The displayed curve is a cubic spline, for which the standard spline()-function of the statistics software R [33] was used. A spline function was used because in principle the measured values are the result of attractive and repulsive interactions. However, the function regarding those interactions depends on physical parameters which were not determined [11]. Therefore a spline function which is based on the fitting of the absolute values and the slope in the data points appeared appropriate to interpolate the measured

data. For the value of the minimum amplitude the optimal dispersant amount was interpolated to be ≈ 0.57 wt%. This amount was used for the batches of all subsequent experiments because the fine fractions were constant for all castables. It was supposed that the dispersant mainly takes effect in the matrix and therefore between the fine particles.

The bulk densities of the green bodies were measured directly after demoulding to analyze the effect of the coarse fraction. Prior to this, the masses were cast and in a first run of the experiments the best flowing mass determined. For a maximum distribution modulus $n_{max} = 0.80$ the only self-flowing castable was obtained. Consequently this mass had the best density-optimized particle size distribution. Presumably friction was overcome because the residual pore volume of the mass was completely filled by the 5 % water. All other masses needed vibration to attain the same flowability. The flowing behaviour was held constant for all batches in the second run by carefully adjusting the vibration amplitude. Fig. 4 shows the influence of the coarse fraction by the distribution modulus n_{max} of the maximum grain size on the measured bulk densities. For $n_{max} = 0.80$, the highest bulk density was achieved.

Figs. 5(a) to 5(d) present the mean values and standard deviations obtained from the complete data sets of the density and porosity measurements after firing. The highest mean density and lowest mean porosity with low standard deviations were obtained for the batch with a maximum distribution modulus $n_{max} = 0.80$. Table 5 summarizes the analyses of variances (ANOVA) for the properties bulk density, open, closed and overall porosity. ANOVA extends the t-test to test at least three means with regard to their statistical significance [34]. The open and closed porosities have a p value exceeding the significance level of 0.05, and therefore for a maximum distribution modulus varying between 0.28 to 1.20, no differences in these properties could be proved (Table 5). On the other hand for the bulk densities and overall porosities the adjusted modulus n_{max} has a significant influence on the means. For this and the following statistical analyses, the software R [33] was used.
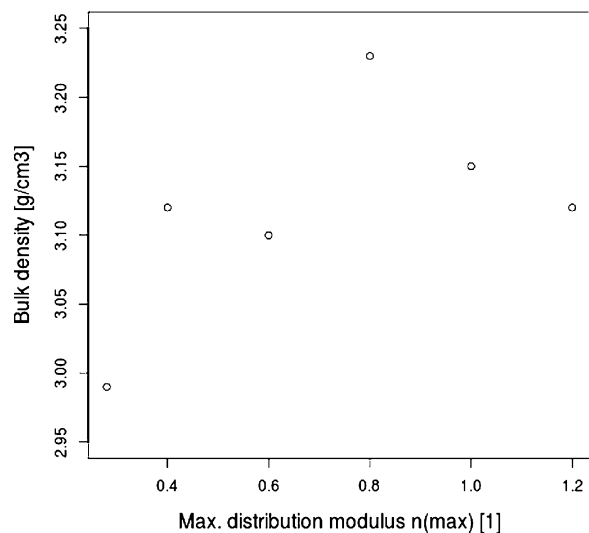

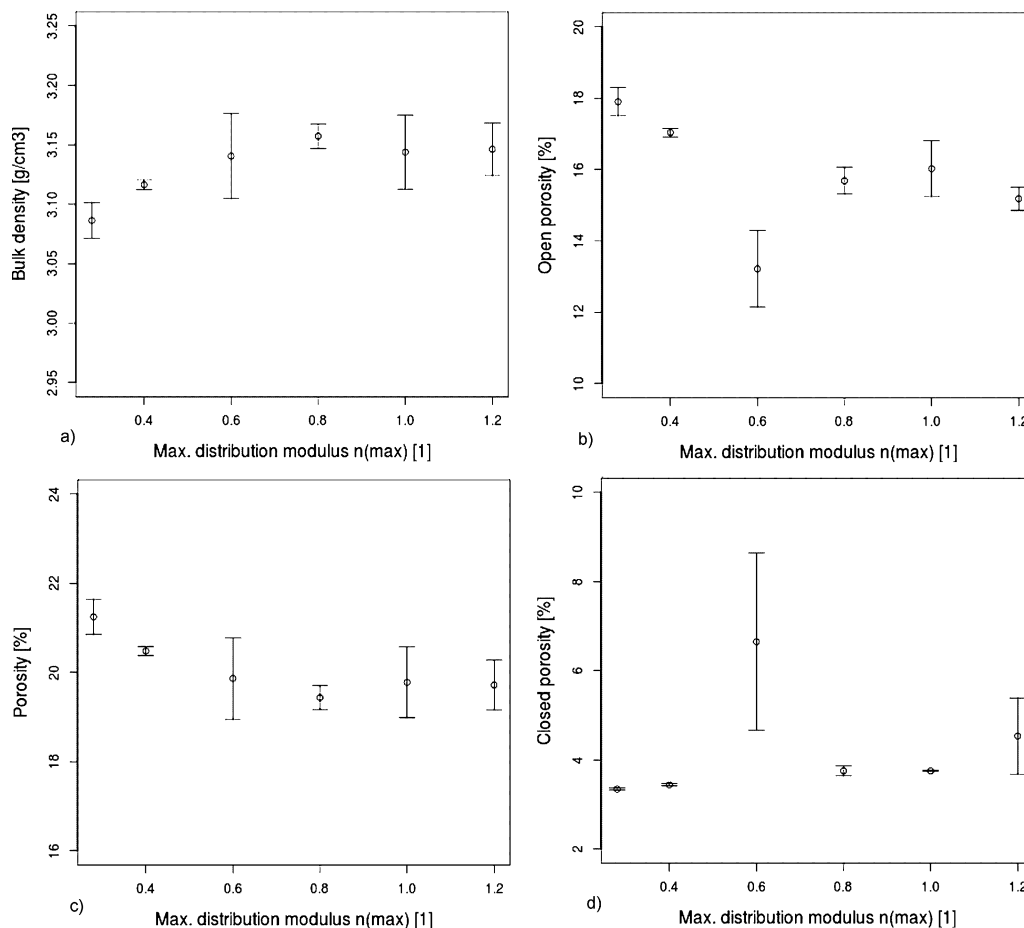**Fig. 4:** Bulk densities of the unfired samples.

Fig. 5: Bulk densities and porosities of the sintered samples. (a) Bulk densities (b) Open porosities (c) Porosities (d) Closed porosities

Table 5: Analyses of variances for the densities and porosities after firing.

Property	Significance	F value	p value
Bulk density	x	10.04	0.00597
Porosity	x	10.04	0.00597
Open porosity		3.334	0.0866
Closed porosity		0.253	0.622

Table 6: Multiple comparisons of the means for the bulk density and porosity for each pair of maximum distribution moduli.

Pairs of moduli n_{max}	Significance	p value for bulk density	p value for porosity
0.28 and 0.40		0.06748	0.06748
0.28 and 0.60		0.1049	0.1049
0.28 and 0.80	x	0.004027	0.004027
0.28 and 1.00		0.06605	0.06605
0.28 and 1.20	x	0.02271	0.02271
0.40 and 0.60		0.3643	0.3643
0.40 and 0.80	x	0.01231	0.01231
0.40 and 1.00		0.2642	0.2642
0.40 and 1.20		0.1408	0.1408
0.60 and 0.80		0.5076	0.5076
0.60 and 1.00		0.9074	0.9074
0.60 and 1.20		0.8275	0.8275
0.80 and 1.00		0.5411	0.5411
0.80 and 1.20		0.4942	0.4942
1.00 and 1.20		0.9212	0.9212

To determine exactly which means are different, the results for each modulus were subject to multiple comparisons with the others. The variances were supposed to be unequal owing to the big differences of the standard deviations in Fig. 5(a) and 5(c). Therefore, as test statistic the two sample t-test for unequal variances (Welch test) was used [34]. The results of the multiple comparisons are presented in Table 6. All porosities range in an interval as small as 19 to 22 % (Fig. 5(c)). Hence also only few pairs are significantly different. The bulk densities and porosities of the samples with $n_{max} = 0.80$ are in any case proven to be different from the ones with $n_{max} = 0.28$ and 0.40. However, the properties for the group of $n_{max} = 0.60$ to 1.20 show no provable differences. It could be concluded that density-optimized packing of the coarse fraction in a range of $n_{max} = 0.60$ to 1.20 led to higher bulk densities and lower porosities (see also mean values in Figs. 5(a) and 5(c)) compared to the samples with $n_{max} = 0.28$ and 0.40. Consequently, in this range (0.60 to 1.20) of the maximum distribution modulus the amount of the coarse

fraction could be freely adjusted. On account of this, for example, the influence of the amount of coarse fraction on other properties such as thermal shock resistance or cold crushing strength could be examined and optimized without significantly changing the bulk densities and porosities.

a)

b)
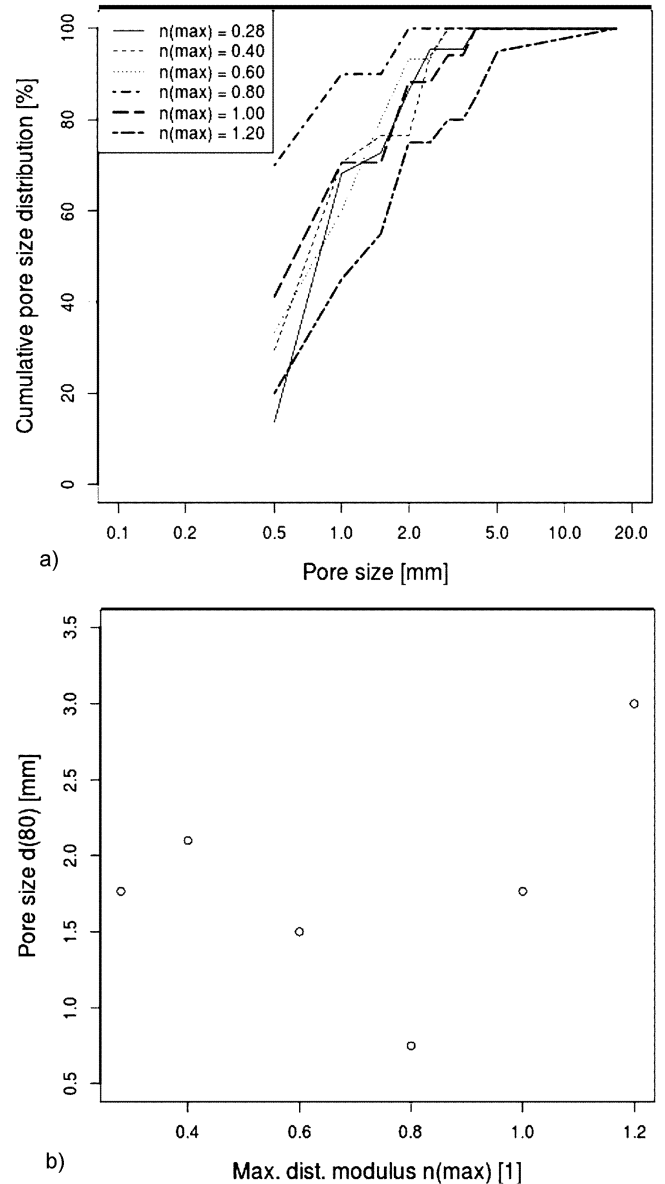
Fig. 6: Pore size range ≥ 500 μm. (a) Cumulative count distribution (b) Pore size d_{80} dependence on n_{max}

Subsequently the pore size distribution experiments were conducted. The cumulative and the related d_{80} graphs for different pore size ranges are plotted in Figs. 6 to Fig. 8. The d_{80} pore sizes are derived from the corresponding cumulative distributions. The d_{80} describes that 80 % of the pores are smaller than this diameter. All three measurements led to different dimensional cumulative distributions (volume, area, count). Therefore for the complete range of pore sizes not one single curve could be plotted. For the interpretation of the pore sizes from the images captured with optical microscopy, the gray values were used to distinguish between pore area and the area of the ceramic body. The lower detection

limit were pore sizes of around ≥ 150 μm. However, especially for large pores ≥ 0.5 mm, the pore areas could not be detected properly owing to an inner structure leading to all possible gray values within the pore (compare Fig. 9). Additionally, for pores as big as the one shown in Fig. 9 the area observed by means of optical microscopy is too small to result in a representative evaluation. Thus in the cumulative area distribution derived from the optical microscopy only pore sizes up to 0.5 mm were considered.

In Fig. 6, it can be seen that the bodies with maximum distribution modulus of 0.8 have the smallest d_{80} with 0.75 mm in the range of the largest pore sizes above 0.5 mm. For lower or higher values of the modulus n_{max} the pore sizes in this size range significantly increase. The largest pores ($d_{80} = 3.0$ mm) were in the batch with $n_{max} = 1.2$. The other maximum distribution moduli led to results for the d_{80} varying from 1.5 to 2.1 mm. Considering that the overall porosities and consequently also the absolute pore volumes vary only slightly (see Fig. 5(c)), it can be supposed that the bodies with $n_{max} = 0.8$ and 0.6 which had the smallest values of the d_{80} in this large pore size range will have higher d_{80} in the ranges of smaller pore sizes.

In the subsequent pore size range of 500 to 150 μm presented in Fig. 7 it can be seen that the d_{80} values are nearly equal (324.9 to 347.3 μm) over the maximum distribution modulus except for $n_{max} = 0.6$ with $d_{80} = 441.2$ μm as expected owing to the comparable overall porosities. However, the batch with a maximum distribution modulus of 0.8 is outstanding because in this pore size range it also shows the lowest d_{80} with 324.9 μm. But therefore it also has the highest d_{80} with 3.7 μm in the pore size range < 150 μm as seen in Fig. 8. As expected, the batches with larger pores in the pore size ranges exceeding 150 μm show lower values for the d_{80} (1.9 to 2.7 μm) in the range < 150 μm.

a)

b)
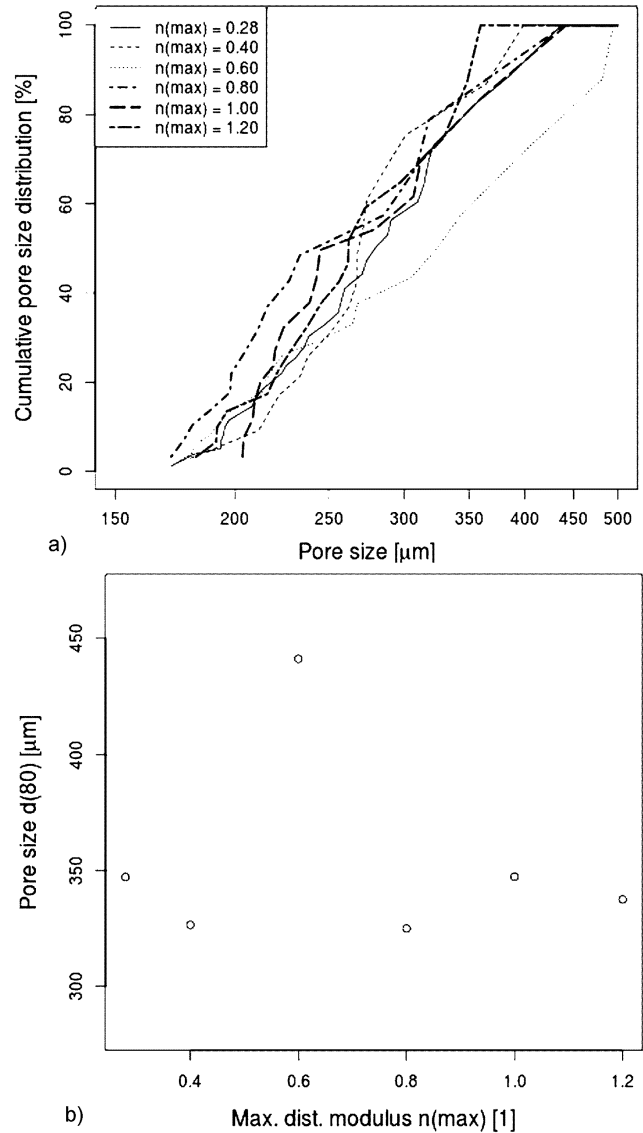
Fig. 7: Pore size range 150 μm to 500 μm. (a) Cumulative area distribution (b) Pore size d_{80} dependence on n_{max}

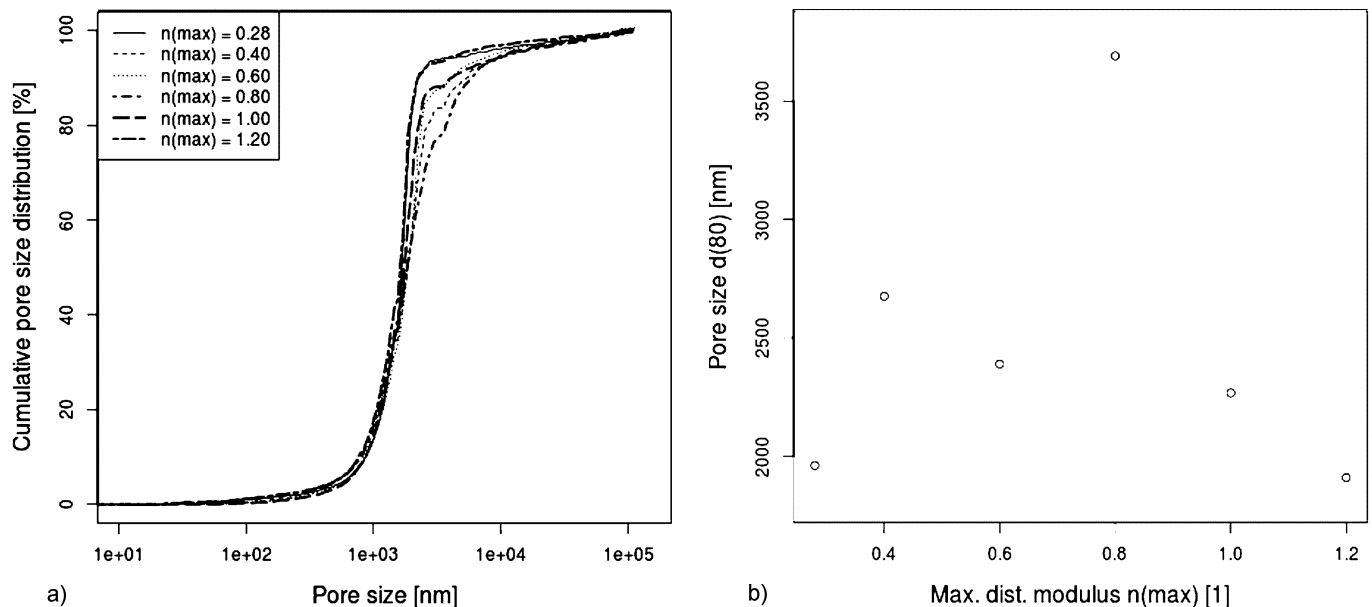
a)   b)

Fig. 8: Pore size range < 150 μm. (a) Cumulative volume distribution (b) Pore size d_{80} dependence on n_{max}
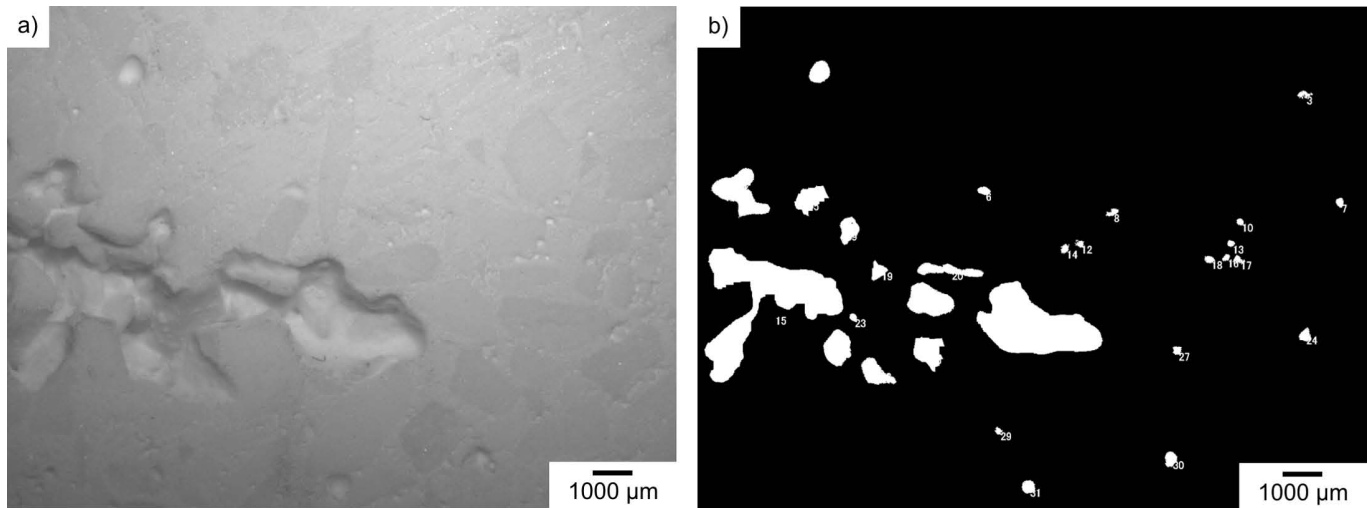
Fig. 9 : Example of limits of optical area detection. (a) Optical microscopy image (20x) (b) Detected pores based on gray value
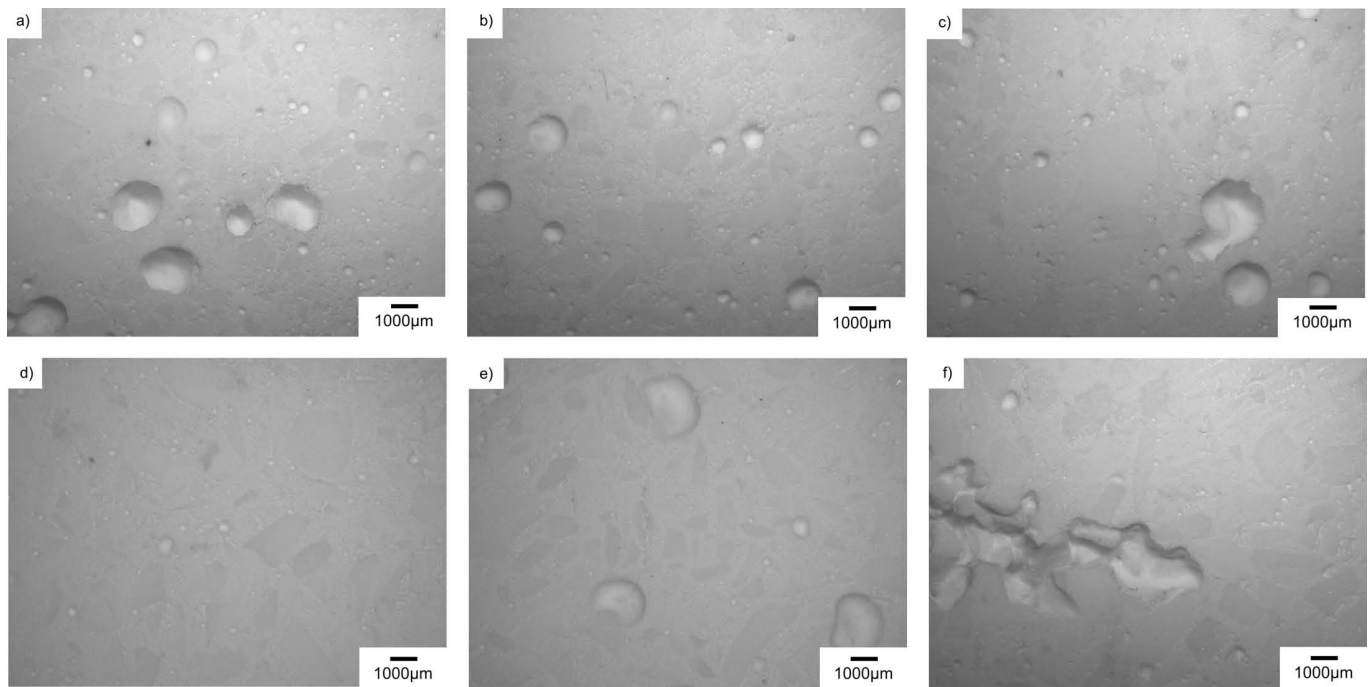

Fig. 10: Optical microscopy images (magnification 20x). (a) n_{max} = 0.28 (b) n_{max} = 0.40 (c) n_{max} = 0.60 (d) n_{max} = 0.80 (e) n_{max} = 1.00 (f) n_{max} = 1.20

It was concluded that for a density-optimized particle size distribution not only flowability and density were improved but also the pore sizes were shifted towards smaller values relative to the full range of pore sizes. The best-optimized refractory was obtained for a maximum distribution modulus of 0.8. Consequently, for lower or higher values of n_{max}, the pore sizes and amounts were increasingly shifted towards larger pore sizes. To prove the measurements and interpretations in Figs. 10 and 11 the optical microscopy images for magnifications of 20x and 50x are presented. The images confirm that the amount and the size of large pores > 150 μm decreased towards a minimum for the body with the maximum distribution modulus of 0.8. Additionally in Fig. 11, the increasing amount of the coarse alumina fraction 1 – 3 mm with increasing

n_{max} is visible as is the reduction of the medium grain sizes between 0.1 – 1 mm. The lubrication layer of fine-grained material between the larger particles can also be seen.

IV. Conclusions

In this work, the influence of the coarse fraction of a particle size distribution on the flowability and density of stable castables was investigated. The Andreasen model was therefore modified such that different distribution moduli could be adjusted for the fine and the coarse fraction. The minimum distribution modulus was held constant at 0.28 for all batches to ensure the stability of the coarse grains. The maximum distribution modulus n_{max} was used as a single parameter to characterize the different coarse fractions and was adjusted between 0.28 to 1.20.
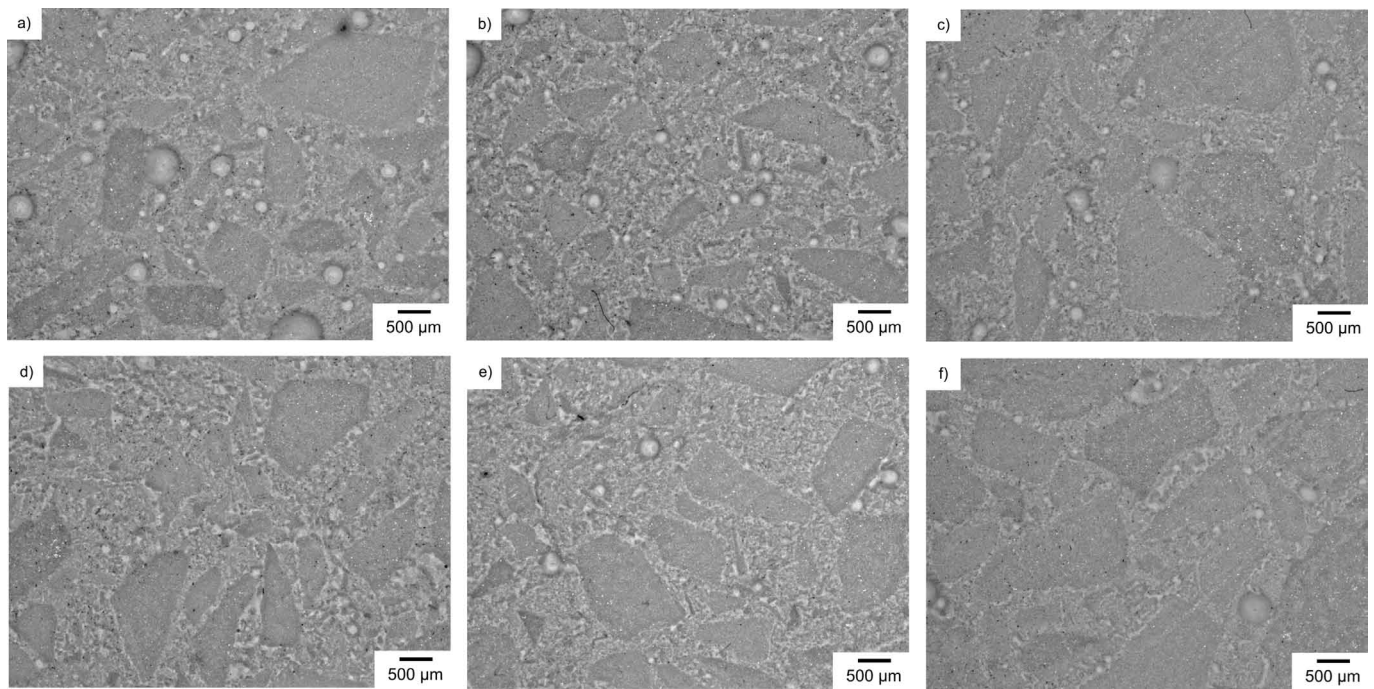
Fig. 11: Optical microscopy images (magnification 50x). (a) $n_{max} = 0.28$ (b) $n_{max} = 0.40$ (c) $n_{max} = 0.60$ (d) $n_{max} = 0.80$ (e) $n_{max} = 1.00$ (f) $n_{max} = 1.20$

The coarse fraction showed an influence on the flowability as the best-flowing castable was obtained for the densest unfired body with $n_{max} = 0.80$. Moreover, density-optimized packing of the coarse fraction in a range of $n_{max} = 0.60$ to 1.20 also led to higher bulk densities and lower porosities of the fired samples compared to the bodies with $n_{max} \leq 0.40$. In the range of the maximum distribution modulus from 0.60 to 1.20, however, no significant differences were seen. On account of this, the influence of the coarse fraction on other properties as thermal shock resistance or cold crushing strength could be examined and optimized without significantly changing the bulk densities and porosities. Furthermore, densest packing in the coarse fraction with $n_{max} = 0.80$ led to the smallest pore sizes relative to the full range of pores. Hence it could be demonstrated that the application of the modified Andreasen model with a minimum distribution modulus < 0.30 for the fine fraction and a density-optimizing one at around 0.80 for the coarse fraction produced a castable with a maximum grain size of 3 mm for which stability, flowability, density and the pore sizes were simultaneously optimized.

Future work should address the adaptability of the modified Andreasen model for other minimum and maximum particle sizes. Therefore the optimum empirical values of the parameters of the distribution moduli could change. The results of the present work on the influence of the coarse fraction on density and pore size distribution could be extended to investigate the influence on other properties such as thermal shock or corrosion resistance. Additionally, an investigation of the relationship of the amount of fines, its size and the stability and flowability of a castable should be interesting as different values for the optimal distribution modulus based on considerations for the fine fraction are recommended in different publications (see Table 1).

References

1 Buhr, A.: Refractories for steel secondary metallurgy, *CN-Refractories*, **6**, [3], 19 – 30, (1999).

2 Peret, C.M., Gregolin, J.A., Faria, L.I.L., Pandolfelli, V.C.: Patent generation and the technological development of refractories and steelmaking, *Refractories Applications and News*, **12**, [1], 10 – 14, (2007).

3 Semler, C.E.: Refractories review 2005 – Update from China, *Refractories Applications and News*, **10**, [4], 6 – 22, (2005).

4 Braulio, M.A.L., Morbioli, G.G., Pandolfelli, V.C.: Advanced boron-containing Al_2O_3-MgO refractory castables, *J. Am. Ceram. Soc.*, **94**, [10], 3467 – 72, (2011).

5 Tomsu, F., Ulbricht, J.: Development trends of the material composition of highly stressed refractory concrete, (in German), *Keramische Zeitschrift*, **50**, [9], 724 – 731, (1998).

6 Feys, D., De Schutter, G., Verhoeven, R.: Parameters influencing pressure during pumping of self-compacting concrete, *Mater. Struct.*, **46**, 533 – 555, (2013).

7 Myhre, B.: Let's make a castable! Part I, *Refractories Applications and News*, **13**, [3], 16 – 24, (2008).

8 Silva, A.P., Segadaes, A.M., Devezas, T.C.: Particle distribution design in a self-flow alumina refractory castable without cement, *Adv. Sci. Tech.*, **45**, 2260 – 2265, (2006).

9 De Larrard, F., Sedran, T.: Optimization of ultra-high-performance concrete by the use of a packing model, *Cement Concrete Res.*, **24**, [6], 997 – 1009, (1994).

[10] Routschka, G.: Refractory materials (in German), Vulkan-Verlag Essen, 2nd edition, 1997.

[11] Reed, J.S.: *Principles of ceramics processing*, 122, 150 ff., 219ff, John Wiley & Sons, Inc., 2nd edition, 1995.

[12] Furnas, C.C.: Grading aggregates I – Mathematical relations for beds of broken solids of maximum density, *Ind. Eng. Chem.*, **23**, [9], 1052 – 1058, (1931).

[13] Andreasen, A.: On the relationship of grading and interstices in products of loose grains, (in German), *Colloid Polym. Sci.*, **50**, 217 – 228, (1930).

[14] Dinger, D.R., Funk, J.E.: Particle packing II – Review of packing of polydisperse particle systems, *Interceram*, **41**, [2], 95 – 97, (1992).

[15] Dinger, D.R., Funk, J.E.: Particle packing IV – Computer modelling of particle packing phenomena, *Interceram*, **42**, [3], 150 – 152, (1993).

[16] Zheng, J., Johnson, P.F., Reed, J.S.: Improved equation of the continuous particle size distribution for dense packing, *J. Am. Ceram. Soc.*, **73**, [5], 1392 – 98, (1990).

[17] Funk, J.E., Dinger, D.R.: *Predictive process control of crowded particulate suspensions*, 327, 507, 566 f. Kluwer Academic Publishers, 1994.

[18] Yu, S.-P., Wang, M.-C., Hon, M.-H.: Properties of alumina-zirconia-raphite refractories with particle size according to the andreasen model, *J. Ceram. Soc. Jpn.*, **108**, [8], 721 – 727, (2000).

[19] Ulbricht, J., Burkhardt, K.: On the grading of coarse ceramic refractory materials, *cfi/Ber.DKG*, **76**, [4], D9 – 12, (1999).

[20] Sudduth, R.D.: A generalized model to predict the viscosity of solutions with suspended particles, I. *J. Appl. Polym. Sci.*, 48, 25 – 36, (1993).

[21] Amaral, M.D., Van Es, S., Asua, J.M.: Effect of the particle size distribution on the low shear viscosity of high-solid-content latexes, *J. Appl. Polym. Sci.: Part A: Polymer chemistry*, **42**, 3936 – 3946, (2004).

[22] Sudduth, R.D.: A generalized model to predict the viscosity of solutions with suspended particles, III. Effects of particle interaction and particle size distribution. *J. Appl. Polym. Sci.*, **50**, 123 – 147, (1993).

[23] Sudduth, R.D.: A generalized model to predict the viscosity of solutions with suspended particles, IV. Determination of optimum particle-by-particle volume fractions, *J. Appl. Polym. Sci.*, **52**, 985 – 996, (1994).

[24] Farris, R.J.: Prediction of the viscosity of multimodal suspensions from unimodal viscosity data, *T. Soc. Rheol.*, **12**, [2], 281 – 301, (1968).

[25] Hoffman, R.L.: Factors affecting the viscosity of unimodal and multimodal colloidal dispersions, *J. Rheol.*, **36**, [5], 947 – 964, (1992).

[26] Pivinskii, Y.E.: Conditions for the complete stability of ceramic slips, *Glass Ceram.*, **28**, [6], 373 – 376, (1971).

[27] Dzuy, N.Q., Boger, D.V.: Yield stress measurement for concentrated suspensions, *J. Rheol.*, **27**, [4], 321 – 349, (1983).

[28] Rhines, F.N.: Dynamic particle stacking. In Onoda, G.Y. and Hench, L.L., editor, Ceramic processing before firing, 321 – 341. John Wiley & Sons, 1978.

[29] Chesters, J.H.: Steelplant refractories – Testing, research and development, 151, The United Steel Companies Ltd., Sheffield, 1957.

[30] Lee, W.E., Zhang, S., Karakus, M.: Refractories: Controlled microstructure composites for extreme environments, *J. Mater. Sci.*, **39**, 6675 – 6685, (2004).

[31] Klippel, U., Aneziris, C.G., Metzger, A.J.: Shaped coarse grained refractories by pressure slip casting, *Adv. Eng. Mater.*, **13**, [1 – 2], 68 – 76, (2011).

[32] Schafföner, S., Aneziris, C.G., Berek, H., Hubalkova, J., Priese, A.: Fused calcium zirconate for refractory applications, *J. Eur. Ceram. Soc.*, **33**, 3411 – 3418, (2013).

[33] R Development Core Team: R: A language and environment for statistical computing, *R Foundation for Statistical Computing, Vienna, Austria, 2010*, ISBN 3 – 900051 – 07 – 0.

[34] Montgomery, D.C.: Design and analysis of experiments, John Wiley & Sons, 5th edition, 2001.